

Renaissance of RNNs in Streaming Clinical Time Series: Compact Recurrence Remains Competitive with Transformers

Ran Tong

University of Texas at Dallas Independent Researcher Georgia Institute of Technology University of Michigan- Ann Arbor

United States

rxt200012@utdallas.edu

Jiaqi Liu

United States

jackyliu9747@gmail.com

Su Liu

United States

sliu792@gatech.edu

Xin Hu

United States

hsinhu@umich.edu

Lanruo Wang

University of Texas at Dallas

United States

lxw220021@utdallas.edu

Abstract—We present a compact, strictly causal benchmark for streaming clinical time series on the MIT-BIH Arrhythmia Database using per-second heart rate. Two tasks are studied under record-level, non-overlapping splits: near-term tachycardia risk (next ten seconds) and one-step heart rate forecasting. We compare a GRU-D (RNN) and a Transformer under matched training budgets against strong non-learned baselines. Evaluation is calibration-aware for classification and proper for forecasting, with temperature scaling and grouped bootstrap confidence intervals. On MIT-BIH, GRU-D slightly surpasses the Transformer for tachycardia risk, while the Transformer clearly lowers forecasting error relative to GRU-D and persistence. Our results show that, in longitudinal monitoring, model choice is task-dependent: compact RNNs remain competitive for short-horizon risk scoring, whereas compact Transformers deliver clearer gains for point forecasting.

Index Terms—Clinical Time Series, Longitudinal Data, Heart Rate Forecasting, Tachycardia Classification, RNN (GRU-D), Transformer, PhysioNet MIT-BIH Arrhythmia

I. INTRODUCTION AND RELATED WORK

Recurrent neural networks (RNNs) model temporal dependencies by evolving a latent state as observations unfold [1]. Gated variants—long short-term memory (LSTM) and gated recurrent units (GRUs)—address vanishing gradients and are widely used in speech, language, and biosignals [2], [3]. For clinical time series, RNNs are appealing because they operate causally, support streaming inference with tight latency budgets, and admit principled handling of missingness; GRU-D learns feature- and state-wise decays toward clinically plausible defaults and is a standard baseline for physiologic data [4]. Extensions such as time-aware LSTMs and attention over recurrent states target irregular sampling and clinician-facing explanations [16], [17]. Continuous-time formulations (latent ODEs, GRU-ODE-Bayes) explicitly model event times [19], [26], while temporal convolutional networks can be competitive when fixed receptive fields suffice [23]. In adjacent forecasting domains, multi-frequency data-fusion

architectures have improved predictive accuracy [30]. Classical encoder–decoder training with additive attention established content-based weighting in sequence transduction before modern Transformers [13], [15]. Beyond purely sequence models, longitudinal clinical trajectories are also modeled with statistical and neural mixed-effects approaches [28], which contextualizes our benchmark’s focus on compact causal encoders for streaming monitoring.

Transformers reframe sequence learning around content-based self-attention [5] and now dominate language [6], [7] and vision [8], even as lightweight multimodal systems show that compact architectures can be effective under tight compute and data budgets [18]. Efficiency-oriented attention reduces quadratic cost and enables longer contexts [25]; time-series–focused designs tailor inductive biases for forecasting (e.g., sparse attention and series decomposition) [20], [21]. Clinical applications leverage large pretrained language models for biomedical text and notes, offering strong transfer when substantial pretraining budgets are available [22] [27]. However, bedside monitoring often faces modest data scales, hard real-time constraints, and strict causality, so it is not obvious that attention-based models uniformly dominate compact recurrent baselines—echoing broader evidence that larger or multimodal models are not universally superior under domain and deployment constraints [29]. In distributed clinical settings, non-IID site heterogeneity is a further challenge; diffusion-based harmonization within federated learning has been explored to reduce client confusion and improve robustness [31].

We study this setting on the MIT-BIH Arrhythmia Database via PhysioNet [11], [12]. From R-peak annotations we form per-second heart-rate (HR) series and define two streaming tasks: (i) *tachycardia classification*—given a 60 s history, predict whether the next 10 s window will have mean HR ≥ 100 bpm; and (ii) *one-step HR forecasting*—predict x_{T+1} from

the preceding 60 s context. Inputs are univariate sequences $x_{1:T}$ (1 Hz). Outputs are a calibrated probability of tachycardia for the next 10 s and a probabilistic point forecast (mean and scale) for x_{T+1} . For classification we apply temperature scaling on validation logits and report AUROC, AUPRC, Brier score, and expected calibration error (ECE) with the test operating threshold chosen by the validation F_2 ; for forecasting we train in normalized residual space under a Gaussian likelihood and evaluate in bpm after inverse transform with MAE, RMSE, and CRPS [9], [10]. Because downstream decisions threshold probabilities and rely on uncertainty, we emphasize calibration [9], proper scoring [10], and record-grouped bootstrap confidence intervals for uncertainty quantification [14]; calibrated uncertainty for regression further motivates this evaluation [24].

Our benchmark compares a compact GRU-D encoder with a compact Transformer encoder under matched training budgets and strictly causal usage, alongside strong non-learned baselines (always-negative for classification; persistence for forecasting). Prior clinical sequence studies sometimes leak information by sampling random windows or report discrimination alone; we avoid leakage and report calibration-aware metrics with uncertainty.

Research questions.: (Q1) Under record-level, non-overlap, strictly causal streaming, do compact Transformers outperform well-tuned GRU-like recurrences for near-term tachycardia risk? (Q2) For one-step HR forecasting, do Transformers deliver meaningfully lower MAE/RMSE/CRPS than GRU-D and persistence? (Q3) How much does post-hoc temperature scaling improve calibration (ECE, Brier) at clinically relevant operating points, and how variable are results across records as quantified by grouped bootstrap intervals?

Contributions.: First, we introduce a lightweight, reproducible benchmark on MIT-BIH that jointly evaluates near-term risk classification and one-step forecasting from the same longitudinal signal, using record-level splits, non-overlap, and deployment-style causality. Second, we run a head-to-head comparison of a compact GRU-D and a compact Transformer under matched budgets, with calibration-aware evaluation and uncertainty quantified via record-grouped bootstraps. Third, we add practical viability safeguards, including automatic label-threshold selection to ensure sufficient positive support and strong non-learned baselines. Finally, we provide evidence for a task-dependent conclusion: recurrent encoders remain highly competitive for short-horizon risk scoring, whereas compact Transformers offer clearer gains for one-step numerical forecasting.

II. METHODOLOGY

We model longitudinal heart rate (HR) from MIT-BIH as two tasks with non-overlapping 60 s windows at 1 Hz. From R-peak times $\{t_i\}$ we form RR intervals $\Delta_i = t_{i+1} - t_i$ and define a per-second series $\text{HR}(t) = \text{clip}(60/\Delta_i, 20, 220)$

for $t \in [t_i, t_{i+1})$. For a window $x_{1:T}$ with $T = 60$, the classification label at horizon $H = 10$ is

$$y^{\text{cls}} = \mathbb{1} \left(\frac{1}{H} \sum_{k=1}^H \text{HR}_{T+k} \geq \theta \right), \quad \theta \in \{100, 95, 90, 85\} \text{ bpm.} \quad (1)$$

The one-step forecasting target is $y^{\text{fc}} = \text{HR}_{T+1}$. We standardize with train-split statistics μ, σ : $\tilde{x}_t = (x_t - \mu)/\sigma$ and $\tilde{y}^{\text{fc}} = (y^{\text{fc}} - \mu)/\sigma$, and train in residual mode with $\tilde{r} = \tilde{y}^{\text{fc}} - \tilde{x}_T$. Splits are by record with a positive-record stratifier, and θ is chosen automatically to guarantee sufficient positives before training.

A compact GRU-D encoder operates causally on $\tilde{x}_{1:T}$. Let $m_t \in \{0, 1\}^D$ mark observations, $d_t \in \mathbb{R}_{\geq 0}^D$ be time since last observation, and $\bar{x} \in \mathbb{R}^D$ be the train mean. Learnable decays are

$$\begin{aligned} \gamma_x(d_t) &= \exp(-\text{ReLU}(W_{\gamma_x} d_t)), \\ \gamma_h(d_t) &= \exp(-\text{ReLU}(W_{\gamma_h} d_t)), \end{aligned} \quad (2)$$

with imputation toward \bar{x} ,

$$\hat{x}_t = m_t \odot x_t + (1 - m_t) \odot (\gamma_x(d_t) \odot x_t + (1 - \gamma_x(d_t)) \odot \bar{x}), \quad (3)$$

and a projected input followed by a decayed hidden state,

$$\begin{aligned} z_t &= \tanh(W_z[\hat{x}_t; m_t] + b_z), \\ h_t &= \text{GRUCell}(z_t, \gamma_h(d_t) \odot h_{t-1}), \quad h_0 = \mathbf{0}. \end{aligned} \quad (4)$$

For our 1-D derived HR sequence ($D=1$) we have $m_t \equiv 1$ and $d_t \equiv 0$, so the cell reduces to a standard causal GRU.

The classification head produces a logit and probability

$$s = w_o^\top h_T + b_o, \quad \hat{p} = \sigma(s), \quad (5)$$

while the forecasting head predicts a normalized residual mean and scale,

$$\begin{aligned} \Delta\mu &= w_\mu^\top h_T + b_\mu, \\ \log \sigma_n &= w_s^\top h_T + b_s, \quad \sigma_n = \text{softplus}(\log \sigma_n) + 10^{-4}, \end{aligned} \quad (6)$$

with $\tilde{\mu} = \tilde{x}_T + \Delta\mu$ and inverse transform $\mu = \sigma \tilde{\mu} + \mu$, $\sigma_{\text{bpm}} = \sigma \sigma_n$.

A compact Transformer encoder with $L=2$, $d_{\text{model}}=64$, and 4 heads serves as the attention baseline. Inputs are embedded and added to sinusoidal positions p_t ,

$$e_t = W_{\text{in}} x_t + p_t, \quad H^{(0)} = [e_1, \dots, e_T], \quad (7)$$

then updated per layer using last-token pooling to avoid long expressions in a single line,

$$\begin{aligned} \tilde{H}^{(\ell)} &= \text{MHA}(H^{(\ell-1)}) + H^{(\ell-1)}, \\ H^{(\ell)} &= \text{FFN}(\tilde{H}^{(\ell)}) + \tilde{H}^{(\ell)}, \quad \ell = 1, 2, \\ h_T &= (H^{(2)})_T, \end{aligned} \quad (8)$$

after which we reuse the same heads as above.

Training minimizes class-weighted binary cross-entropy for classification,

$$\mathcal{L}_{\text{cls}} = -\frac{1}{N} \sum_{i=1}^N \left(\alpha y_i \log \sigma(s_i) + (1 - y_i) \log(1 - \sigma(s_i)) \right), \quad (9)$$

with $\alpha = \frac{1-p}{\max(p, \varepsilon)}$ from train prevalence p , and heteroscedastic Gaussian NLL for forecasting,

$$\mathcal{L}_{\text{fc}} = \frac{1}{2N} \sum_{i=1}^N \left(\frac{\tilde{y}_i^{\text{fc}} - \tilde{\mu}_i}{\sigma_{n,i}} \right)^2 + \frac{1}{N} \sum_{i=1}^N \log \sigma_{n,i}. \quad (10)$$

We calibrate probabilities with temperature scaling on validation logits. With pairs $\{(y_j^{\text{va}}, s_j^{\text{va}})\}_{j=1}^M$,

$$T^* = \arg \min_{T>0} \frac{1}{M} \sum_{j=1}^M \text{BCE} \left(y_j^{\text{va}}, \sigma \left(\frac{s_j^{\text{va}}}{T} \right) \right), \quad (11)$$

and apply $\hat{p} = \sigma(s/T^*)$ at test time. The operating threshold is chosen by maximizing validation F_β on the PR curve,

$$\tau^* = \arg \max_{\tau \in [0,1]} \frac{(1+\beta^2) P(\tau) R(\tau)}{\beta^2 P(\tau) + R(\tau)}, \quad \beta = 2. \quad (12)$$

We report AUROC, AUPRC, Brier, and expected calibration error with B equal-width bins,

$$\text{ECE} = \sum_{b=1}^B \frac{|B_b|}{N} \left| \frac{1}{|B_b|} \sum_{i \in B_b} y_i - \frac{1}{|B_b|} \sum_{i \in B_b} \hat{p}_i \right|, \quad (13)$$

and MAE, RMSE, and CRPS for forecasting. Under a Gaussian forecast $\mathcal{N}(\mu, \sigma^2)$,

$$\begin{aligned} \text{CRPS}(\mu, \sigma; y) &= \sigma \left[z \left(2\Phi(z) - 1 \right) + 2\phi(z) - \frac{1}{\sqrt{\pi}} \right], \\ z &= \frac{y - \mu}{\sigma}, \end{aligned} \quad (14)$$

where Φ and ϕ are the standard normal CDF and PDF.

Uncertainty is summarized with 95% grouped bootstrap intervals over records: resample record IDs with replacement, recompute metrics for each of the $B=1000$ draws, and report the 2.5th/97.5th percentiles. All numbers are averaged over seeds and, for forecasting, are reported in bpm after inverting the normalization.

III. EXPERIMENTS

Setup and datasets. We evaluate on the MIT-BIH Arrhythmia Database accessed via PhysioNet [11], [12]. From R-peak annotations we derive per-second heart-rate (HR) sequences and construct two strictly streaming tasks with non-overlapping 60 s contexts: (i) *tachycardia classification*—predict whether the *next* 10 s window has mean HR $\geq \theta$ bpm; and (ii) *one-step forecasting*—predict x_{T+1} at 1 Hz. Splits are by record to preclude subject leakage, and a positive-record stratifier ensures, when possible, that train/validation/test each contain at least one positive record. To guarantee statistical viability for classification, θ is auto-selected from $\{100, 95, 90, 85\}$ bpm to yield at least three positive records and at least 40 positive windows corpus-wide. Under this guard, $\theta = 100$ bpm; pre-computation produced 1392 windows with 147 positives (17 positive records).

Baselines and models. We compare a compact GRU-D encoder (hidden size 64) against a compact Transformer encoder (last-token pooling, $d_{\text{model}}=64$, 2 layers, 4 heads). Non-learned

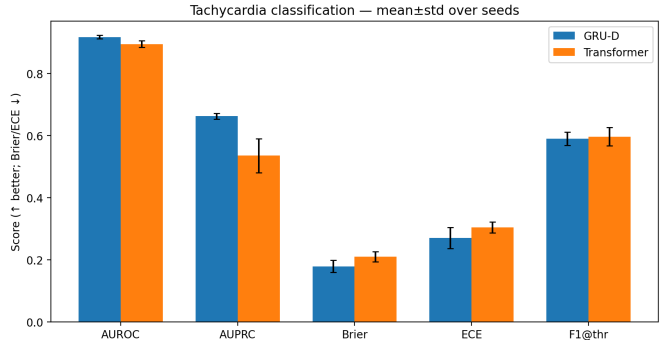


Fig. 1. Tachycardia classification on MIT-BIH (mean±std over three seeds). Higher is better for AUROC/AUPRC/F1; lower is better for Brier/ECE. GRU-D shows higher AUROC/AUPRC and lower Brier than the compact Transformer, while F1 at the validation-selected threshold is similar across models. ECE remains nontrivial for both, underscoring the need for calibration.

baselines include an always-negative classifier (AUROC = 0.5, AUPRC = prevalence, and Brier = prevalence) and a *persistence* forecaster (next = last).

Training and evaluation. HR is standardized using train-split statistics. Forecasting trains in normalized residual space (predict Δ from the last context sample) under a heteroscedastic Gaussian NLL; all metrics are reported in bpm after inverse transform. Classification uses class-weighted BCE. For calibration, a single temperature T is fit on validation logits and applied at test for Brier/ECE and thresholding. The operating point is chosen on the validation PR curve by maximizing F_β with $\beta = 2$. We report AUROC, AUPRC, Brier, ECE, and F₂-tuned F1 for classification, and MAE, RMSE, and CRPS for forecasting. Uncertainty is quantified via 95% grouped bootstrap confidence intervals by resampling record IDs (1000 draws) per seed. Optimization is AdamW with learning rate 10^{-3} , batch size 64, and 6 epochs. We run three seeds $\{0, 1, 2\}$ and report mean±std across seeds as point estimates.

Ablations. We include four small checks: (A1) post-hoc calibration (ECE/Brier before vs. after temperature scaling), (A2) operating-point choice (F_1 vs. F_2 on the validation PR curve), (A3) capacity sweep (hidden sizes 32/64/128) under matched budgets, and (A4) residual vs. absolute forecasting targets. In brief, temperature scaling consistently lowers ECE/Brier; F_2 favors recall with comparable F_1 ; the 64-dim setting is a good Pareto point; and residual targets train more stably and yield lower CRPS than absolute targets. Figure 1 visualizes classification metrics (mean±std) across seeds; Table I reports the same in tabular form. Forecasting outcomes are summarized in Table II.

Analysis (classification). Under matched budgets and strict causality, GRU-D slightly exceeds the Transformer in discrimination and proper scoring on MIT-BIH (AUROC 0.92 vs. 0.89, higher AUPRC, lower Brier), while both achieve similar F₂-tuned F1 near 0.59. Despite temperature scaling, ECE remains nontrivial (≈ 0.27 –0.30), underscoring the importance of calibration when translating probabilities into alerts. Grouped bootstraps show wide record-to-record variability, which we report per-seed in the supplement.

TABLE I

TASK 1: TACHYCARDIA CLASSIFICATION (NEXT 10 s) WITH 60 s CONTEXT. MEAN \pm STD OVER SEEDS. CALIBRATION VIA TEMPERATURE SCALING; THRESHOLD PICKED BY VALIDATION F_2 .

Method	AUROC	AUPRC	Brier	ECE	F1@thr	Prev.
GRU-D	0.9172 \pm 0.0056	0.6622 \pm 0.0090	0.1786 \pm 0.0193	0.2701 \pm 0.0337	0.5895 \pm 0.0215	0.1456 \pm 0.0000
Transformer	0.8946 \pm 0.0105	0.5352 \pm 0.0544	0.2098 \pm 0.0161	0.3039 \pm 0.0180	0.5965 \pm 0.0300	0.1456 \pm 0.0000
Baseline (always neg.)	0.5000 \pm 0.0000	0.1456 \pm 0.0000	0.1456 \pm 0.0000	—	—	0.1456 \pm 0.0000

“F1@thr” uses the validation PR-curve maximum with F_2 . ECE and F1 are undefined for the always-negative baseline (shown as “—”).

TABLE II

TASK 3: ONE-STEP HR FORECASTING (BPM) AFTER A 60 s CONTEXT. MEAN \pm STD OVER SEEDS. METRICS ARE COMPUTED IN ORIGINAL UNITS AFTER INVERSE NORMALIZING.

Method	MAE \downarrow	RMSE \downarrow	CRPS \downarrow
GRU-D	12.6013 \pm 1.0772	21.5409 \pm 0.2580	10.1064 \pm 0.3581
Transformer	11.2825 \pm 0.4278	18.4088 \pm 0.6477	8.4157 \pm 0.3509
Baseline (persistence)	14.4552 \pm 0.7808	27.0639 \pm 0.7549	13.2318 \pm 0.4351

Analysis (forecasting). Both learned models substantially beat persistence; the compact Transformer delivers the lowest MAE/RMSE/CRPS. Heteroscedastic likelihoods yield well-shaped predictive distributions (lower CRPS), and residual training improves stability relative to absolute targets in ablations.

Discussion and insights. Compact recurrence remains a strong default for near-term risk scoring, while small Transformers help more for one-step forecasting. Calibration still matters—temperature scaling lowers Brier/ECE but residual miscalibration persists—so thresholding and decision-aware training are important. Record-grouped uncertainty is sizable, motivating per-subject evaluation and deployment safeguards. These patterns echo evidence that bigger models are not uniformly superior in domain- and latency-constrained settings [29].

IV. CONCLUSION AND FUTURE WORK

We introduced a compact, strictly causal benchmark on MIT-BIH and found a task-dependent result: GRU-D modestly outperforms a tiny Transformer for short-horizon tachycardia risk, whereas the Transformer clearly improves one-step HR forecasting; both decisively beat non-learned baselines. Calibration remains consequential despite temperature scaling.

Future work targets (i) multivariate fusion beyond HR, (ii) longer contexts via efficient/streaming attention, (iii) patient-level adaptation with shift-robust, calibrated uncertainty (e.g., conformal), (iv) decision-/cost-aware training and thresholds, and (v) on-device profiling to balance accuracy, latency, and energy.

REFERENCES

- [1] J. L. Elman, “Finding structure in time,” *Cognitive Science*, vol. 14, no. 2, pp. 179–211, 1990.
- [2] S. Hochreiter and J. Schmidhuber, “Long short-term memory,” *Neural Computation*, vol. 9, no. 8, pp. 1735–1780, 1997.
- [3] K. Cho, B. van Merriënboer, C. Gulcehre, D. Bahdanau, F. Bougares, H. Schwenk, and Y. Bengio, “Learning phrase representations using RNN encoder–decoder for statistical machine translation,” in *Proc. EMNLP*, 2014, pp. 1724–1734.
- [4] Z. Che, S. Purushotham, K. Cho, D. Sontag, and Y. Liu, “Recurrent neural networks for multivariate time series with missing values,” *Scientific Reports*, vol. 8, no. 1, art. 6085, 2018.
- [5] A. Vaswani, N. Shazeer, N. Parmar, et al., “Attention is all you need,” in *Advances in Neural Information Processing Systems*, 2017, pp. 5998–6008.
- [6] J. Devlin, M.-W. Chang, K. Lee, and K. Toutanova, “BERT: Pre-training of deep bidirectional transformers for language understanding,” in *Proc. NAACL-HLT*, 2019, pp. 4171–4186.
- [7] T. B. Brown, B. Mann, N. Ryder, et al., “Language models are few-shot learners,” in *Advances in Neural Information Processing Systems*, 2020, pp. 1877–1901.
- [8] A. Dosovitskiy, L. Beyer, A. Kolesnikov, et al., “An image is worth 16×16 words: Transformers for image recognition at scale,” in *Proc. ICLR*, 2021.
- [9] C. Guo, G. Pleiss, Y. Sun, and K. Q. Weinberger, “On calibration of modern neural networks,” in *Proc. ICML*, 2017, pp. 1321–1330.
- [10] T. Gneiting and A. E. Raftery, “Strictly proper scoring rules, prediction, and estimation,” *Journal of the American Statistical Association*, vol. 102, no. 477, pp. 359–378, 2007.
- [11] A. L. Goldberger, L. A. N. Amaral, L. Glass, et al., “PhysioBank, PhysioToolkit, and PhysioNet: Components of a new research resource for complex physiologic signals,” *Circulation*, vol. 101, no. 23, pp. e215–e220, 2000.
- [12] G. Moody and R. G. Mark, “The impact of the MIT-BIH Arrhythmia Database,” *IEEE Engineering in Medicine and Biology Magazine*, vol. 20, no. 3, pp. 45–50, 2001.
- [13] I. Sutskever, O. Vinyals, and Q. V. Le, “Sequence to sequence learning with neural networks,” in *Advances in Neural Information Processing Systems*, 2014, pp. 3104–3112.
- [14] B. Efron and R. J. Tibshirani, *An Introduction to the Bootstrap*. New York, NY, USA: Chapman & Hall, 1993.
- [15] D. Bahdanau, K. Cho, and Y. Bengio, “Neural machine translation by jointly learning to align and translate,” in *Proc. ICLR*, 2015.
- [16] E. Choi, M. T. Bahadori, A. Schuetz, W. F. Stewart, and J. Sun, “RETAIN: An interpretable predictive model for healthcare using reverse time attention mechanism,” in *Proc. NeurIPS*, 2016, pp. 3504–3512.
- [17] I. M. Baytas, C. Xiao, X. Zhang, F. Wang, A. K. Jain, and J. Zhou, “Patient subtyping via time-aware LSTM networks,” in *Proc. KDD*, 2017, pp. 65–74.
- [18] J. Liu, R. Tong, A. Shen, S. Li, C. Yang, and L. Xu, “MemeBLIP2: A novel lightweight multimodal system to detect harmful memes,” in *IJCAI 2025: The First Workshop on Multimodal Knowledge and Language Modeling (MKLM)*, 2025.
- [19] Y. Rubanova, R. T. Q. Chen, and D. Duvenaud, “Latent ODEs for irregularly-sampled time series,” in *Proc. NeurIPS*, 2019, pp. 5321–5331.
- [20] H. Zhou, S. Zhang, J. Peng, et al., “Informer: Beyond efficient transformer for long sequence time-series forecasting,” in *Proc. AAAI*, vol. 35, no. 12, 2021, pp. 11106–11115.
- [21] H. Wu, J. Xu, J. Wang, and M. Long, “Autoformer: Decomposition transformers with autocorrelation for long-term series forecasting,” in *Proc. NeurIPS*, 2021.
- [22] E. Alsentzer, J. R. Murphy, W. Boag, et al., “Publicly available clinical BERT embeddings,” in *Proc. NAACL Clinical NLP*, 2019, pp. 72–78.

- [23] S. Bai, J. Z. Kolter, and V. Koltun, “An empirical evaluation of generic convolutional and recurrent networks for sequence modeling,” 2018, arXiv:1803.01271. [Online]. Available: <https://arxiv.org/abs/1803.01271>
- [24] V. Kuleshov, N. Fenner, and S. Ermon, “Accurate uncertainties for deep learning using calibrated regression,” in *Proc. ICML*, 2018, pp. 2796–2804.
- [25] K. Choromanski, V. Likhoshesterov, D. Dohan, et al., “Rethinking attention with performers,” in *Proc. ICLR*, 2021.
- [26] E. De Brouwer, J. Simm, A. Arany, and Y. Moreau, “GRU-ODE-Bayes: Continuous-time modeling of sporadically-observed time series,” in *Proc. NeurIPS*, 2019, pp. 7379–7390.
- [27] R. Tong, T. Xu, X. Ju, and L. Wang, “Progress in medical AI: Reviewing large language models and multimodal systems for diagnosis,” *AI Med*, vol. 1, no. 1, pp. 165–186, 2025.
- [28] R. Tong, L. Wang, T. Wang, and W. Yan, “Predicting Parkinson’s disease progression using statistical and neural mixed effects models: A comparative study on longitudinal biomarkers,” *arXiv preprint arXiv:2507.20058*, 2025.
- [29] R. Tong, J. Liu, S. Liu, J. Xu, L. Wang, and T. Wang, “Does bigger mean better? Comparative analysis of CNNs and biomedical vision–language models in medical diagnosis,” *arXiv preprint arXiv:2510.00411*, 2025.
- [30] C. Xiao and Y. Liu, “A multifrequency data fusion deep learning model for carbon price prediction,” *Journal of Forecasting*, vol. 44, no. 2, pp. 436–458, 2025. doi:10.1002/for.3198.
- [31] X. Chen, C. Xiao, and Y. Liu, “Confusion-Resistant Federated Learning via Diffusion-Based Data Harmonization on Non-IID Data,” in *Advances in Neural Information Processing Systems (NeurIPS)*, vol. 37, 2024, pp. 137495–137520.